

## A hybrid extended finite element/level set method for modeling phase transformations

H. Ji<sup>1</sup>, D. Chopp<sup>2</sup> and J. E. Dolbow<sup>1,\*†</sup>

<sup>1</sup>*Department of Civil and Environmental Engineering, Duke University, Durham, NC 27708, U.S.A.*

<sup>2</sup>*Engineering Science and Applied Mathematics, Northwestern University, Evanston, IL 60208, U.S.A.*

### SUMMARY

A hybrid numerical method for modelling the evolution of sharp phase interfaces on fixed grids is presented. We focus attention on two-dimensional solidification problems, where the temperature field evolves according to classical heat conduction in two subdomains separated by a moving freezing front. The enrichment strategies of the eXtended Finite Element Method (X-FEM) are employed to represent the jump in the temperature gradient that governs the velocity of the phase boundary. A new approach with the X-FEM is suggested for this class of problems whereby the partition of unity is constructed with  $C^1(\Omega)$  polynomials and enriched with a  $C^0(\Omega)$  function. This approach leads to jumps in temperature gradient occurring only at the phase boundary, and is shown to significantly improve estimates for the front velocity. Temporal derivatives of the temperature field in the vicinity of the phase front are obtained with a projection that employs discontinuous enrichment. In conjunction with a finer finite difference grid, the Level Set method is used to represent the evolution of the phase interface. An iterative procedure is adopted to satisfy the constraints on the temperature field on the phase boundary. The robustness and utility of the method is demonstrated with several benchmark problems of phase transformation. Copyright © 2002 John Wiley & Sons, Ltd.

KEY WORDS: X-FEM; sharp interface; phase transformations; level set

### 1. INTRODUCTION

Phase boundaries represent diffuse material interfaces across which several fields may exhibit sharp gradients, and even discontinuities as the interface thickness vanishes and becomes ‘sharp’. A wide range of numerical methods have been developed for these classes of problems according to the pertinent physics and assumptions about the interface. We refer the reader to Reference [1] for a review (see also Reference [2]). When a sharp interface is assumed, its motion is governed by the jump in the temperature gradient normal to the phase boundary, and is accompanied by a release in latent heat. Additional constraints may be placed at the interface, such as the classical Gibbs–Thomson relations describing the unstable dendritic

\*Correspondence to: J. E. Dolbow, Department of Civil and Environmental Engineering, Pratt School of Engineering, Duke University, Box 90287, Durham, North Carolina 27708-0287, U.S.A.

†E-mail: jdolbow@duke.edu

growth of crystals into an undercooled melt. In order to satisfy these conditions, the most common numerical approaches for sharp interfaces explicitly track the motion of the interface. Within the interface tracking approach, two general divisions can be discerned; moving mesh methods and mixed Eulerian–Lagrangian or fixed grid methods.

Moving finite element mesh methods conform element boundaries to the phase interface as it evolves. Perhaps the most popular method is the use of continuously deforming elements developed by Lynch and O’Neill [3]. Although the method does tend to be very accurate, it is limited by the severe mesh distortion that eventually occurs in two- and three-dimensional problems. Its use has therefore primarily been for directional solidification problems, and in particular for cases where the freezing front remains relatively planar and stable. Sampath and Zabarar [4] provide a recent adaptation of the method along these lines. An alternative ALE approach based on the same method was presented in Ghosh and Moorthy [5], but user control was still required to prevent mesh distortion.

To alleviate these difficulties, a number of Eulerian–Lagrangian methods have been developed recently that track the interface while solving the equations on a fixed grid. These include the immersed interface method [6] and the immersed boundary technique [2]. An excellent review of these methods as well as a new approach can be found in Reference [7]. Importantly, many of these methods effectively smear the discontinuity over a few grid cells, and are therefore not capable of representing the true discontinuity at the phase interface. Although the work of Udaykumar *et al.* [7] provides a significant improvement, the method requires extensive modifications to the finite difference stencil near the interface. Moreover, it does not appear to provide a simple means to address merging and bifurcating interfaces.

A new approach for representing localized behaviour has recently emerged in the finite element literature, termed the partition of unity method [8]. The main idea is to extend a classical approximation by augmenting the set of nodal shape functions with products of a subset of these same shape functions and local enrichment functions. The eXtended Finite Element Method (X-FEM) [9, 10] is a variation on this framework that seeks to model arbitrarily evolving geometric features (such as cracks and interfaces) with evolving enrichment functions. The origins of the method can be traced back to the minimal remeshing method proposed by Belytschko and Black [11]. The enrichment functions may be selected using either specific information about the local solution (i.e. order of singularity) or general information (i.e. degree of continuity). The underlying mesh that is employed to construct the partition of unity remains fixed in the method, while the sets of enrichment functions evolve with the crack or interface geometry. Based upon the work of Daux *et al.* [12] and Dolbow [10] for representing intersecting discontinuities, the concept of discontinuous enrichment was generalized by Belytschko *et al.* [13]. The X-FEM has been employed to simulate crack growth without remeshing for both two-dimensional [9, 14] and three-dimensional problems [15]. Finally, we note that the method shares many common elements with the Generalized Finite Element Method [16, 17].

Recently, the X-FEM has been coupled to the Level Set method as a means of representing interface and crack topologies. Sukumar *et al.* [18] first employed the hybrid technique to model arbitrary fixed material interfaces and voids. The coupled method has been applied to both two-dimensional [19] and three-dimensional [20] quasi-static crack evolution. The pairing of the methods has proven to be particularly advantageous, as evolving functions are employed to capture both the geometry and the local solution of the moving crack front. The approach shares some common traits with the work of Rao *et al.* [21] who employed a Galerkin

Least-Squares level set method in conjunction with the enhanced discontinuous interpolations of Simo *et al.* [22]. The hybrid X-FEM/Level Set method differs in two important respects; (1) a finite difference method is retained for the non-linear advection equation, preserving the vital connection to hyperbolic conservation laws and enabling the use of narrow band techniques; and (2) the enriched approximation is conforming, and the X-FEM does not belong to the class of assumed strain methods. Importantly, there are no free parameters in the hybrid method.

In the present paper, the application of the hybrid X-FEM/LSM to two-dimensional solidification problems is presented. The application of the method is the first one to focus on a time dependent, non-linear problem formulation. It is largely based on previous work with the X-FEM for modelling problems with evolving heat sources and phase boundaries [23, 24]. Importantly, the enrichment strategies of the X-FEM allow for the representation of a sharp interface on the finite element grid. For representing arbitrary gradient discontinuities, we present a new argument and some numerical examples in the present paper to justify the use of a smooth  $C^1(\Omega)$  partition of unity in conjunction with a  $C^0(\Omega)$  enrichment. Through the examination of several example problems, we demonstrate how the present method provides for excellent accuracy in simulating phase boundary evolution, without recourse to remeshing.

During the review process for the present paper, our attention was called to a similar effort by Chessa *et al.* [25] employing level sets with the X-FEM for Stefan problems. Although the work shares several common features with that presented herein, the differences (aside from the choice of continuity in the basis) are worth elucidating. In the first instance, the upwinding scheme we use in the finite difference method for the level set update does not involve any free stabilization parameters. Secondly, the type of problems involving sharp interfaces inevitably involve an evaluation of the jump in field gradient at the phase boundary. In Reference [25], this quantity is obtained by post-processing the X-FEM approximation, whereas the present work determines the jump in heat flux at the interface in a manner that is energetically consistent. The distinction is important, as previous efforts with finite elements for Stefan-like problems have demonstrated how post-processing the approximation can lead to overall conservation imbalance [26].

This paper is organized as follows. In Section 2, we provide the problem formulation for the general case of transient thermal analysis with an embedded phase boundary. The discretization with the X-FEM and the construction of the enrichment functions are then described in Section 3. The weak formulation of the BVP and the current time-stepping algorithm are also described. Section 4 describes the use of the level set method to evolve the geometry of the phase interface. The results from several numerical examples are then provided in Section 5. Finally, Section 6 provides a summary and some concluding remarks.

## 2. PROBLEM FORMULATION

We begin by considering the domain  $\Omega$  which is divided into the regions  $\Omega_1$  and  $\Omega_2$  by the phase interface  $\Gamma_1$  as shown in Figure 1. In the context of solidification problems, we will designate  $\Omega_1$  and  $\Omega_2$  as the regions for the solid and liquid phases, respectively. A zoom of the interface is shown in Figure 2. We seek to determine the evolution of the

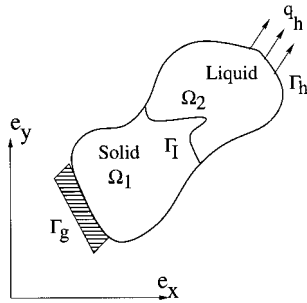


Figure 1. Domain split into  $\Omega_1$  and  $\Omega_2$  by the surface  $\Gamma_I$ .

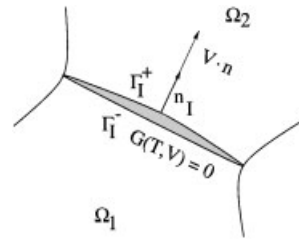


Figure 2. Zoom of the interface  $\Gamma_I$ .

temperature field

$$T : \Omega \times \mathbb{I} \rightarrow \mathcal{R} \tag{1}$$

over the time interval  $t \in \mathbb{I} = (0, t_f)$ . The field satisfies the governing equations, boundary and initial conditions, and constraints on the interface. The governing equations are given by

$$c_1 T_{,t} = \nabla \cdot (\kappa_1 \cdot \nabla T) \quad \text{in } \Omega_1 \tag{2a}$$

$$c_2 T_{,t} = \nabla \cdot (\kappa_2 \cdot \nabla T) \quad \text{in } \Omega_2 \tag{2b}$$

where  $c_1, c_2$  are the volumetric heat capacities of the phases, and  $\kappa_1, \kappa_2$  are the thermal conductivity tensors. The above are supplemented with external boundary conditions and an initial condition

$$T = T_g \quad \text{on } \Gamma_g \times \mathbb{I} \tag{3a}$$

$$-(\kappa \cdot \nabla T) \cdot \mathbf{n} = q_h \quad \text{on } \Gamma_h \times \mathbb{I} \tag{3b}$$

$$T|_{t=0} = T_0 \tag{3c}$$

with  $T_g$  and  $q_h$  prescribed temperatures and heat fluxes, respectively. In the above,  $\mathbf{n}$  denotes the unit outward normal to the domain.

The evolution of the surface  $\Gamma_I$  is described by a *Stefan* condition, written as

$$V_n(\mathbf{x}_I) = \frac{\bar{q}}{L} \tag{4}$$

where  $L$  is the volumetric latent heat of fusion, and  $V_n$  is the normal velocity at a point  $\mathbf{x}_I$  on the interface. The equation arises by considering the localization of the conservation of energy onto the surface of discontinuity  $\Gamma_I$ , and involves the jump in interfacial heat flux

$$\bar{q} = (\kappa_1 \cdot \nabla T)|_{\Gamma_I^-} \cdot \mathbf{n}_I - (\kappa_2 \cdot \nabla T)|_{\Gamma_I^+} \cdot \mathbf{n}_I \tag{5}$$

where we have adopted the convention of describing the liquid side of the interface as positive, and the solid side as negative. We will see that this is consistent with the level set implementation described in Section 4. In the above, the normal vector to the interface  $\mathbf{n}_l$  is assumed to point into the liquid phase.

Additional constraints may be prescribed on the phase boundary  $\Gamma_1$ , which we write in the general form

$$\mathcal{G}(T, V_n, G) = 0 \quad \text{on } \Gamma_1 \tag{6}$$

where  $G$  consists of geometric quantities such as curvature and normal orientation. Examples include the classical Gibbs–Thomson relations for the unstable dendritic growth of crystals into an undercooled melt. In the present investigation, we consider the equality constraint given by

$$\mathcal{G}(T, V_n, G) = T - T_m \quad \text{on } \Gamma_1 \tag{7}$$

where  $T_m$  is the melting temperature. This completes the description of the boundary value problem we wish to solve.

### 3. DISCRETIZATION WITH THE X-FEM

In this section, we provide a summary of the X-FEM approach to the two-dimensional problem described in the previous section. The key issues include the enriched approximation and the time-stepping algorithm. Modifications to standard time-stepping schemes are required due to the nature of the enriched approximation. As this was addressed in detail in Reference [24], we provide only a summary of the algorithm herein. Our intention is to focus on the enrichment strategy, as it is markedly different from those advocated previously.

#### 3.1. The enriched approximation

We consider the space of weighting functions given by

$$\mathcal{V} = \{w : w \in H^1(\Omega), w = 0 \text{ on } \Gamma_g\}$$

and the solution space

$$\mathcal{U} = \{T : T \in H^1(\Omega), T = T_g \text{ on } \Gamma_g\}$$

A standard Galerkin approximation begins by considering a finite dimensional subspace  $\mathcal{V}^h$  spanned by  $N$  linearly independent functions of the weighting space  $\mathcal{V}$ . For the sake of concreteness, we now consider a rectangular domain  $\Omega$  and a regular finite element triangulation  $\mathcal{T}^h = \bigcup_{e=1}^{nel} \mathcal{T}_e$  such that  $\mathcal{T}^h = \Omega$  as shown in Figure 3(a). This figure also depicts an interface whose geometry  $\Gamma_1$  is taken to be independent of the mesh. A standard finite element basis for  $\mathcal{V}^h$  is constructed from the space of complete polynomials  $P^k(\mathcal{T}_e^h)$  of order  $\leq k$  over each element:

$$\mathcal{V}^h = \text{span}\{\phi_i\}_{i=1}^N \quad \text{where } \{\phi_i \in C^0(\mathcal{T}^h) : \phi_i|_{\mathcal{T}_e^h} \in P^k(\mathcal{T}_e^h) \text{ and } \phi_i|_{\Gamma_g} = 0\} \tag{8}$$

where the functions  $\phi_i(\mathbf{x})$  are typically the nodal shape functions. Any linear combination of these functions results in a continuous interpolation for the temperature field, and thus

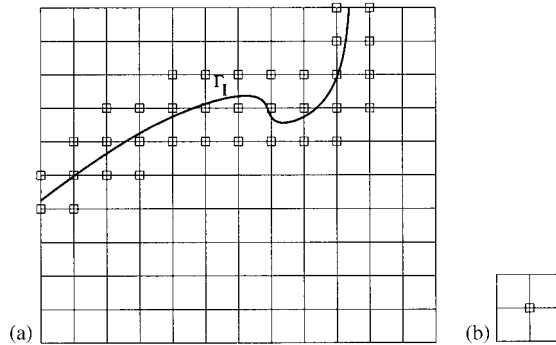


Figure 3. (a) An arbitrary phase interface placed on a mesh. The shape functions of the squared nodes form a partition of unity for enrichment. (b) The support of a single nodal shape function.

possesses poor approximation properties for representing arbitrary discontinuities. Several finite element approaches construct moving meshes that conform to the interface geometry in order to represent the gradient discontinuity.

The X-FEM takes an alternative approach by *extending* the standard finite element approximation. We consider the set of overlapping subdomains  $\{\omega_i\}$  defining the support of each nodal shape function (shown in Figure 3(b)) and sets of enrichment functions  $\{\mathcal{E}_i^k\}$  that possess desirable approximation properties over each subdomain. The method follows the *partition-of-unity* framework [8] through multiplying the enrichment functions by the nodal shape functions  $\phi_i$  in order to ensure a conforming approximation. A general X-FEM basis for  $\mathcal{V}^h$  is therefore

$$\mathcal{V}^h = \text{span} \left\{ \{\phi_i\} \cup \{\phi_i \mathcal{E}_i^k\}_{k=1}^{N_i^E} \right\}_{i=1}^N \tag{9}$$

where  $N$  is the number of standard nodal shape functions and  $N_i^E$  is the number of enrichment functions for node  $i$ . The approximation to the temperature field  $T(\mathbf{x})$  is then written as

$$T(\mathbf{x}) = \sum_i a_i \phi_i(\mathbf{x}) + \sum_i \phi_i(\mathbf{x}) \left( \sum_k \mathcal{E}_i^k \mathcal{E}_i^k(\mathbf{x}) \right) \tag{10}$$

where the  $a_i$  and  $\mathcal{E}_i^k$  are the constant degrees of freedom. It bears emphasis that as a consequence of the above construction, the coefficients  $a_i$  are *not* equal to the value of the temperature field  $T^h(\mathbf{x}_i)$  at the nodes.

The above construct is the most general form of the X-FEM approximation where every nodal shape function may be enriched with an arbitrary number of additional functions  $\{\mathcal{E}_i^k\}_{k=1}^{N_i^E}$ . In practice, only those functions whose supports are in the vicinity of a feature of interest are enriched, giving the approximation a local character. For example, an enriched approximation for a phase interface can be written as

$$T^h(\mathbf{x}) = \underbrace{\sum_{i \in I} a_i \phi_i(\mathbf{x})}_{\text{classical approximation}} + \underbrace{\sum_{j \in J} e_j \phi_j(\mathbf{x}) g(\mathbf{x})}_{\text{enrichment}} \tag{11}$$

where  $I$  is the set of all nodes in the mesh and  $J$  is the set of nodes that form a partition of unity for the function  $g(\mathbf{x})$ . We define this set as

$$J = \{j \in I : \omega_j \cap \Gamma_1 \neq \emptyset\}$$

and use  $N^E$  to denote the size of the set. As shown in Figure 3, only those nodes in the vicinity of the interface are selected; the X-FEM extends a standard finite element approximation locally.

Examining the gradient of the enriched approximation,

$$\nabla T^h(\mathbf{x}) = \sum_{i \in I} a_i \nabla \phi_i(\mathbf{x}) + \sum_{j \in J} e_j (\nabla \phi_j(\mathbf{x}) g(\mathbf{x}) + \phi_j(\mathbf{x}) \nabla g(\mathbf{x})) \tag{12}$$

reveals that gradient discontinuities will arise in the approximation for the temperature field wherever they exist in the enrichment function. As a result, arbitrary material interfaces can be modelled through the use of an enrichment function with discontinuous derivatives. This was precisely the argument employed in both Reference [27] and later in Reference [18] for stationary material interfaces.

The problem with the above construct for moving material interfaces and  $C^0(\Omega)$  shape functions  $\{\phi_i\}$  concerns the additional derivative discontinuities across element boundaries. These may lead to a loss in accuracy as the interface approaches element boundaries, as explored in Reference [18]. An additional concern involves the possibility for linear dependencies in the approximation, especially with piecewise linear enrichment functions that resemble the classical chapeau functions.

In the present investigation, we explore the use of  $C^1(\Omega)$  continuous functions to construct the partition of unity. For the uniform meshes used in this initial study, it is relatively easy to construct two-dimensional Hermite interpolants by taking the tensor product of the one-dimensional interpolants:

$$\begin{aligned} M_i^{00} &= H^0(\xi, \xi_i) \cdot H^0(\eta, \eta_i), & M_i^{01} &= H^0(\xi, \xi_i) \cdot H^1(\eta, \eta_i) \\ M_i^{10} &= H^1(\xi, \xi_i) \cdot H^0(\eta, \eta_i), & M_i^{11} &= H^1(\xi, \xi_i) \cdot H^1(\eta, \eta_i) \end{aligned} \tag{13}$$

where  $(\xi, \eta)$  are the parent co-ordinates on the biunit square. The nodal co-ordinates in the parent domain  $(\xi_i, \eta_i)$  are given by the  $i$ th corner of  $[-1, 1] \times [-1, 1]$ . The one-dimensional  $C^1$  Hermite functions are then

$$H^0(\xi, \xi_i) = -\frac{\xi_i}{4}(\xi + \xi_i)^2(\xi - 2\xi_i), \quad H^1(\xi, \xi_i) = \frac{1}{4}(\xi + \xi_i)^2(\xi - \xi_i) \tag{14}$$

and similarly for  $H^0(\eta, \eta_i)$  and  $H^1(\eta, \eta_i)$ .

It is easy enough to show that the functions  $\{M_i^{00}\}$  alone form a  $C^1$  partition of unity subordinate to the cover  $\{\omega_i\}$ . On an element level, the enriched approximation for the temperature field then takes the form:

$$T^h(\mathbf{x}(\xi)) = \sum_{i=1}^4 (M_i^{00} a_i + M_i^{01} b_i + M_i^{10} c_i) + \sum_{j \in J^e} M_j^{00} e_j g(\mathbf{x}(\xi)) \tag{15}$$

where  $J^e$  denotes the subset of element nodes in the enriched set  $J$ . Importantly, we will only employ regular meshes of 4 node quads such as shown in Figure 3, so that the above will be strictly  $C^1(\Omega)$ , even after mapping the  $\{M_j^{kl}\}$  to the global co-ordinates. We note that this is

less a restriction with the X-FEM than for other numerical methods, as the method provides a means to model irregular domains with uniform meshes, cf. Reference [12]. Moreover, with a rectangular mesh it is not necessary to include the functions  $M_i^{11}$  to insure global continuity or linear precision, and so we have not included these basis functions. Finally, a possible alternative  $C^1(\Omega)$  approximation on unstructured meshes concerns that recently proposed in Reference [28].

Adopting a relatively simple  $C^0(\Omega)$  ‘plateau’ function for  $g(\mathbf{x})$ ,

$$g(\mathbf{x}) = \begin{cases} 1 & \mathbf{x} \in \Omega_1 \\ 1 - \|\mathbf{x} - \mathbf{x}_1\| & \mathbf{x} \in \Omega_2 \end{cases} \quad (16)$$

where  $\mathbf{x}_1$  is the closest point to  $\Gamma_1$  from  $\mathbf{x}$ , yields the following expression for the jump in temperature derivative on the interface:

$$[[\nabla T^h(\mathbf{x})]]_{\Gamma_1} = \sum_{j \in J} M_j^{00} e_j [[\nabla g(\mathbf{x})]]_{\Gamma_1} \quad (17)$$

where the jump operator on  $\Gamma_1$  is given by  $[[f]] = f^+ - f^-$  with  $f^\pm|_{\mathbf{x}_1} = \lim_{\varepsilon \rightarrow 0} f(\mathbf{x}_1 \pm \varepsilon \mathbf{n}_1)$ . The gradient discontinuity is therefore entirely contained within the enrichment function. As a result, it is relatively easy to demonstrate that the products  $M_j^{00} g(\mathbf{x})$  are linearly independent of the functions  $\{M_j^{kl}\}$ .

In what follows, we will find it convenient to adopt an independent approximation for the time derivative of the temperature field. In particular, as the field  $T_{,t}(\mathbf{x})$  is expected to be discontinuous across the phase boundary, we will employ an approximation of the form:

$$T_{,t}^n(\mathbf{x}(\xi)) = \sum_{i=1}^4 (M_i^{00} a_i + M_i^{01} b_i + M_i^{10} c_i) + \sum_{j \in J^e} M_j^{00} e_j H(\mathbf{x}) \quad (18)$$

where the generalized Heaviside function is given by

$$H(\mathbf{x}) = \begin{cases} 0 & \mathbf{x} \in \Omega_1 \\ 1 & \mathbf{x} \in \Omega_2 \end{cases}$$

Both this enrichment function and Equation (16) are easily constructed with the aid of the level set function (see Section 4).

### 3.2. Weak formulation and time-stepping

We briefly describe the two-dimensional analog to the weak formulation/time stepping algorithm presented in Reference [24]. We consider the solution on the time interval  $[0, t_f]$ , partitioned into time steps as  $[t^n, t^{n+1}]$ . Allowing for discontinuous properties across  $\Gamma_1$ , we write (2) at time step  $t^{n+1}$  as

$$cT_{,t}^{n+1} = \nabla \cdot (\mathbf{\kappa} \nabla T)^{n+1} \quad \text{on } \Omega_1, \Omega_2 \quad (19)$$

and we consider the generalized trapezoidal time-stepping algorithm characterized by the parameter  $\alpha$ :

$$T_{,t}^{n+1} = \frac{T^{n+1} - T^n - (1 - \alpha)\Delta t T_{,t}^n}{\alpha \Delta t} \quad (20)$$

After substituting into the above, multiplying by an arbitrary weighting function and integrating by parts, we obtain the following weak form:

$$(w, cT^{n+1})_{\Omega} + \alpha\Delta t B(w, T^{n+1}) - \alpha\Delta t (w, \bar{q}^{n+1})_{\Gamma_1} = (w, cT^n)_{\Omega} + (1 - \alpha)\Delta t (w, cT_{,t}^n)_{\Omega} \quad (21)$$

where we have assumed that  $\Gamma_h = \emptyset$  for simplicity. In the above,  $(\cdot, \cdot)_{\Theta}$  denotes the  $L_2$  inner product over the domain  $\Theta$ , and

$$B(w, T^{n+1}) = (\nabla w, \mathbf{\kappa} \cdot \nabla T)_{\Omega} \quad (22)$$

We note that the above equations explicitly involve the time derivative of the temperature field, as first introduced with the X-FEM for hyperbolic problems by Gerlach [29]. With a standard formulation, these are obtained in a straightforward fashion once the new temperature field is determined via (20). With a semi-discrete approach, the above leads to an expression for the time derivative of the temperature at each node. This is not possible with the enriched approximation (11), as the set  $J$  is not fixed in time. We therefore perform an  $L^2$  projection of the form

$$(w, T_{,t}^{n+1})_{\Omega} = \left( w, \frac{T^{n+1} - T^n - (1 - \alpha)\Delta t T_{,t}^n}{\alpha\Delta t} \right)_{\Omega} \quad (23)$$

to determine the field  $T_{,t}^{n+1}$ . Importantly, this projection can be restricted to the set of elements with enriched nodes at time steps  $t^n$  and  $t^{n+1}$ . We note that similar projections are often employed in space–time formulations [30].

We now provide a brief description of the time-stepping algorithm. Knowing quantities at time step  $t^n$ , we can determine the position of the interface at time step  $t^{n+1}$  using the Level Set method described in Section 4. We then solve for the temperature field at the new time step,  $T^{n+1}$ , using (21) and for its time derivative, using (23). Rather than explicitly solving for the interface fluxes at  $t^{n+1}$  by substituting (5) into the above, we adopt a standard iterative procedure described in the appendix. This will enable us to determine the jump in interface flux such that the constraint (7) is satisfied.

### 3.3. Matrix equations and summary of the algorithm

A staggered strategy is employed to solve the coupled problem of advecting the interface position with the evolving temperature field. We suppose that the temperature field, position of the interface, and jump in interface flux at time step  $t^n$  are known. We calculate the velocity of the interface  $V_I^n$  using (4), and predict the position of the interface at time  $t^{n+1}$  using the Level Set method as described in Section 4.

In the following, we denote the set of classical basis functions by

$$\Phi_i = \{M_i^{00}, M_i^{01}, M_i^{10}\}$$

and the enriched basis functions by  $\Psi_i = M_i^{00}g$ . The algorithm proceeds as follows:

1. We build the global matrix equations. These result from substituting the approximation (15) into the discrete form of (21) and invoking the arbitrariness of the weight functions. The resulting system of equations reads

$$(\mathbf{M} + \alpha\Delta t\mathbf{K})\mathbf{d}_0^{n+1} = \mathbf{F}_0^{n+1} \quad (24)$$

where

- The vector of classical and enriched degrees of freedom:

$$\mathbf{d}_0^{n+1} = \left\{ \{a_i, b_i, c_i\}_{i=1}^N, \{e_j\}_{j=1}^{N^E} \right\}^T \quad (25)$$

- Mass matrix:

$$\mathbf{M} = \begin{bmatrix} \mathbf{M}_1 & \mathbf{M}_2 \\ \mathbf{M}_3 & \mathbf{M}_4 \end{bmatrix} \quad (26)$$

where the entries of the above are given by

$$[\mathbf{M}_1]_{ij} = (\Phi_i, c\Phi_j)_\Omega, \quad [\mathbf{M}_2]_{ij} = (\Phi_i, c\Psi_j^{n+1})_\Omega \quad (27a)$$

$$[\mathbf{M}_3]_{ij} = (\Psi_i^{n+1}, c\Phi_j)_\Omega, \quad [\mathbf{M}_4]_{ij} = (\Psi_i^{n+1}, c\Psi_j^{n+1})_\Omega \quad (27b)$$

- Stiffness matrix:

$$\mathbf{K} = \begin{bmatrix} \mathbf{K}_1 & \mathbf{K}_2 \\ \mathbf{K}_3 & \mathbf{K}_4 \end{bmatrix} \quad (28)$$

where the entries of the above are given by

$$[\mathbf{K}_1]_{ij} = B(\Phi_i, \Phi_j), \quad [\mathbf{K}_2]_{ij} = B(\Phi_i, \Psi_j^{n+1}) \quad (29a)$$

$$[\mathbf{K}_3]_{ij} = B(\Psi_i^{n+1}, \Phi_j), \quad [\mathbf{K}_4]_{ij} = B(\Psi_i^{n+1}, \Psi_j^{n+1}) \quad (29b)$$

- Forcing term:

$$\mathbf{F}_0 = \begin{bmatrix} \mathbf{F}_1 \\ \mathbf{F}_2 \end{bmatrix} \quad (30)$$

with

$$[\mathbf{F}_1]_i = (\Phi_i, cT^n)_\Omega + (1 - \alpha) \cdot \Delta t (\Phi_i, cT_t^n)_\Omega \quad (31a)$$

$$[\mathbf{F}_2]_i = (\Psi_i^{n+1}, cT^n)_\Omega + (1 - \alpha) \cdot \Delta t (\Psi_i^{n+1}, cT_t^n)_\Omega \quad (31b)$$

In the above, the temperature field at time step  $t^n$  is obtained from (15). The time derivative of the temperature is obtained from (18), with the constant coefficients  $\{a_i, b_i, c_i\}$  and  $e_j$  determined from the projection, whose matrix form is provided below in (32).

2. A standard iteration procedure (see the appendix) is performed so that the interfacial condition is satisfied and the jump in heat flux  $\bar{q}^{n+1}$  is determined at each point on the interface.
3. The temperature field and fluxes at the new time step are stored. We perform the  $L^2$  projection to determine the time derivatives of the temperature field for the new time

step. The matrix equations for this operation are given by

$$\mathbf{\Pi s} = \boldsymbol{\tau} \tag{32}$$

where

- the vector of unknowns:

$$\mathbf{s} = \{\{a_i, b_i, c_i\}, \{e_j\}\}^T \tag{33}$$

- the projection matrix:

$$\mathbf{\Pi} = \begin{bmatrix} \mathbf{\Pi}_1 & \mathbf{\Pi}_2 \\ \mathbf{\Pi}_3 & \mathbf{\Pi}_4 \end{bmatrix} \tag{34}$$

with

$$[\mathbf{\Pi}_1]_{ij} = (\Phi_i, \Phi_j)_\Omega, \quad [\mathbf{\Pi}_2]_{ij} = (\Phi_i, \Psi_j^{n+1})_\Omega \tag{35a}$$

$$[\mathbf{\Pi}_3]_{ij} = (\Psi_i^{n+1}, \Phi_j)_\Omega, \quad [\mathbf{\Pi}_4]_{ij} = (\Psi_i^{n+1}, \Phi_j^{n+1})_\Omega \tag{35b}$$

- the history term

$$\boldsymbol{\tau} = \begin{bmatrix} \boldsymbol{\tau}_1 \\ \boldsymbol{\tau}_2 \end{bmatrix} \tag{36}$$

with

$$[\boldsymbol{\tau}_1]_i = \frac{1}{\alpha \Delta t} (\Phi_i, T^{n+1} - T^n - (1 - \alpha) \Delta t T_t^n)_\Omega \tag{37a}$$

$$[\boldsymbol{\tau}_2]_i = \frac{1}{\alpha \Delta t} (\Psi_i^{n+1}, T^{n+1} - T^n - (1 - \alpha) \Delta t T_t^n)_\Omega \tag{37b}$$

We note that for the time projection, the enriched basis functions are  $\Psi_i = M_i^{00} H$ .

4. The position of the interface at the next time  $t^{n+1}$  is found with the aid of the Level Set method described in Section 4. This process involves
  - Building the extension velocity field on the domain given the velocity of the phase boundary calculated from (4) and the heat fluxes  $\bar{q}^{n+1}$  found in step 2. This procedure is facilitated by the Fast Marching Method.
  - Solving the non-linear advection equation to determine the position of the interface at  $t^{n+2}$ .
5. We return to the first step and the algorithm repeats.

*Remarks*

1. A large portion of the mass (26) and stiffness matrix (28) consist of the terms  $\mathbf{M}_1$  and  $\mathbf{K}_1$ , respectively. These entries only need to be evaluated at the first time step.
2. The projection is only required for elements with enriched nodes. On the rest of the domain, (20) can be used to obtain the time derivatives of the temperature in terms of the nodal coefficients  $a_i^n$  and  $a_i^{n+1}$ .

3. The algorithm avoids the need to calculate the gradients at the interface by obtaining the jump in interface flux  $\bar{q}$  during the iterative procedure. Importantly, these fluxes are consistent with the weak form (21), and using them to move the interface through (4) conserves energy.
4. In the absence of constraints on a phase boundary, step 2 may be skipped entirely.

### 3.4. Numerical integration

As the geometry of the interface  $\Gamma_1$  is independent of the mesh with the X-FEM, it is necessary to modify the quadrature routines used to assemble the volume integrals in (21). The matrix system of equations arising from the discrete weak form is normally constructed with a loop over all elements, as the domain is approximated by

$$\bar{\Omega} = \bigcup_{e=1}^m \bar{\Omega}_e \quad (38)$$

where  $m$  is the number of elements, and  $\bar{\Omega}_e$  is the element subdomain. For elements intersected by the phase interface, we define the element subdomain to be a union of a set of subpolygons whose boundaries align with the interface geometry:

$$\bar{\Omega}_e = \bigcup_{e=1}^{m_{es}} \bar{\Omega}_{es} \quad (39)$$

where  $m_{es}$  denotes the number of subpolygons for the element.

In earlier investigations for crack growth, each side of an intersected element was recursively triangulated to form a set of subtriangles. As the subtriangles conformed to the crack geometry, this approach resulted in an accurate integration of the discontinuity in the enriched basis. However, when the interface is translating across the element, this approach becomes very expensive due to the need to assemble the discrete forms of the integrals

$$(w, cT^{n+1}), \quad (w, cT^n)$$

The interface may generally be located at two different positions at  $t^n$  and  $t^{n+1}$ , and so one of these terms will contain multiple derivative discontinuities, depending on when the weight function is constructed.

We therefore adopt a slightly different approach, choosing instead to partition cut elements into subquadrilaterals as shown in Figure 4. This technique was proposed in Reference [10] and results in a more efficient integration scheme, particularly when the interface is translating across elements. While the subquadrilaterals do not necessarily conform to the local geometry, the integration error can be sufficiently bounded by choosing enough divisions. For the present investigation, we use 5 divisions in each direction. These subpolygons are also used to determine which nodes are enriched with the interface function  $g(\mathbf{x})$ , by calculating the percentage of a node's support 'above' and 'below' the interface.

To construct the surface integrals on the interface, it is necessary to discretize  $\Gamma_1$ . The procedure is directly analogous to the one adopted in Reference [31]. We first divide  $\Gamma_1$  into one-dimensional segments. The segments are determined according to the interaction of the level set function with the mesh as illustrated in Figure 5. This latter operation is described

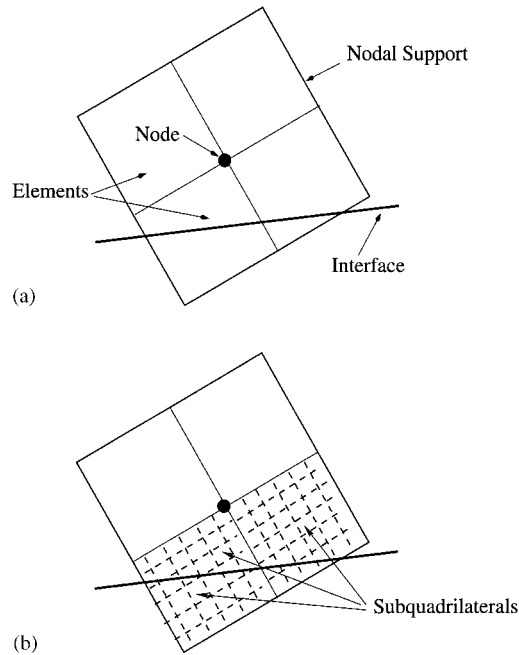


Figure 4. (a) Nodal support intersected by a phase boundary; (b) the subquadrilaterals associated with elements intersected by the interface used for enriched node selection and the assembly of element stiffness matrices.

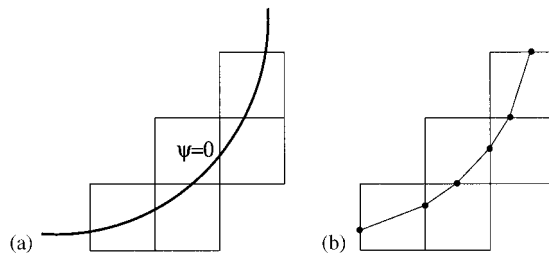


Figure 5. (a) Intersection of zero level set surface with the mesh; (b) one-dimensional segments used for integration.

in detail in Reference [18]. A set of one-dimensional subelements along  $\Gamma_1$  results. These subelements are similar to the two-dimensional subpolygons used for the volume integrals, in that no new degrees of freedom are associated with their generation.

## 4. EVOLVING THE INTERFACE WITH LEVEL SETS

Given a geometric description of the phase interface and its velocity at time step  $t^n$ , we wish to determine its evolution. In the Level Set method [32], the interface is represented as the zero level surface of a function of one higher dimension. The main advantages of this approach are that topological changes are handled naturally without special cases, it is easily extended to any number of spatial dimensions, and the underlying numerical methods are based on well established finite difference methods for hyperbolic conservation laws enabling the accurate and stable evolution of sharp corners and cusps in the interface. We give here a brief overview of the Level Set method.

Imagine a closed curve  $\Gamma$  in the plane propagating normal to itself with speed  $V_n$ . We can embed the initial position of the front as the zero level set of a higher dimensional function  $\psi$ , and then identify the evolution of this function  $\psi$  with the propagation of the front itself through a time-dependent initial value problem. At any time, the front is given by the zero level set of the time-dependent level set function  $\psi$ . In order to derive an equation of motion for this level set function  $\psi$ , we stipulate that the zero level set of the evolving function  $\psi$  always match the propagating interface which means that

$$\psi(\mathbf{x}(t), t) = 0 \quad (40)$$

By the chain rule,

$$\psi_{,t} + \nabla\psi(\mathbf{x}(t), t) \cdot \mathbf{x}'(t) = 0 \quad (41)$$

Since  $V_n$  supplies the speed in the outward normal direction, then  $\mathbf{x}'(t) \cdot \mathbf{n} = V_n$  where  $\mathbf{n} = \nabla\psi / \|\nabla\psi\|$  and this yields an evolution equation for  $\psi$ , namely,

$$\begin{aligned} \psi_{,t} + V_n \|\nabla\psi\| &= 0 \\ \psi(\mathbf{x}, t=0) &\text{ given} \end{aligned} \quad (42)$$

This is the level set equation introduced in Reference [32].

As analysed in Reference [33], the efficient solution of these front propagation problems requires the use of upwind difference schemes and schemes borrowed from the solution of hyperbolic conservation laws. A detailed discussion of such schemes in the context of interface propagation may be found in Reference [34]. In the present context, we note that the finite difference stencil employed for the level set equations is not required to coincide with the finite element stencil used to assemble (24). The coupling of the two systems ((21) and (42)) proceeds entirely from the calculation of the interface velocity  $V_n$ .

One of the drawbacks to the level set approach is its requirement that the speed function  $V_n$  be given in the entire domain of  $\psi$ . This information is not always available. This is the case in here, where the speed  $V_n$  of the interface is known only at the interface, not on the entire domain of  $\psi$ . Fortunately, there is a technique for taking a speed  $V_n$  known on the interface only and extending it in a reasonable way to  $V_n^{\text{ext}}$  on the rest of the domain. That technique is based upon the fast marching method described below. Once the extended velocity field is computed, the interface is advanced through (42). After applying (42), the new location of the interface is extracted from  $\psi$  by use of bicubic interpolation on each element of the mesh which has a change in sign among its nodal values (indicating the presence of the interface) [35].

#### 4.1. The fast marching method

In the context of the Level Set method, the Fast Marching Method was introduced in Reference [36], and later improved in References [37, 35]. We will use this method to construct the extended velocity field described above. We begin by rewriting the level set equation as

$$\psi_t + V_n^{\text{ext}} \|\nabla\psi\| = 0 \quad (43)$$

where  $V_n^{\text{ext}}$  is some velocity field which agrees with the speed function  $V_n$  which is defined on the zero level set,

$$V_n^{\text{ext}}|_{\psi=0} = V_n \quad (44)$$

This new velocity field  $V_n^{\text{ext}}$  is known as the ‘extension velocity’. In Reference [38], a technique for building  $V_n^{\text{ext}}$  from  $V_n$  in a highly efficient and accurate manner is given. This technique relies on the Fast Marching Method.

Briefly, the Fast Marching Method solves an equation of the form

$$\|\nabla\phi\| = \frac{1}{F(\mathbf{x})} \quad (45)$$

by first replacing the gradient by suitable upwind operators, and then systematically advancing the front by marching outwards from the boundary data in an upwind fashion. The key to the algorithm lies in the observation that an upwind operator implies a causality, and hence grid points with a given value for  $\phi$  cannot be affected by those with a larger value. Hence, as the solution is advanced, we maintain a heap sort which keeps track of the smallest element to be updated, and thus always advances the solution ‘downwind’ of that point. Through the use of this sorting algorithm, each point in the domain is visited *only once*, rather than requiring any iteration; the resulting technique has a total operation count of  $O(N \log N)$  where  $N$  is the number of nodes.

This technique is used to construct the extension velocity  $V_n^{\text{ext}}$  by computing the signed distance function  $\phi$  (obtained by letting  $F(x, y) = 1$  in (45)) while simultaneously solving the associated equation

$$\nabla V_n^{\text{ext}} \cdot \nabla\phi = 0 \quad (46)$$

with the same upwind finite differences. The resulting velocity field  $V_n^{\text{ext}}$  satisfies (44) and also adds stability to the Level Set method by maintaining

$$\|\nabla\psi\| = 1 \quad (47)$$

almost everywhere. The signed distance function  $\phi$  constructed here is also used to evaluate the expression  $\|\mathbf{x} - \mathbf{x}_1\|$  in the enrichment function (16), and to determine points in  $\Omega_1$  or  $\Omega_2$  for  $H(\mathbf{x})$ . For a complete description of the Fast Marching Method as implemented in this paper, see Reference [35].

## 5. NUMERICAL EXAMPLES

## 5.1. Two-phase Stefan problem

The classical Stefan problem models the one-dimensional freezing of a semi-infinite ( $y > 0$ ) domain. The problem is essentially one-dimensional, but we solve it here in two dimensions to illustrate the salient features of the method. The initial temperature  $T_0(\mathbf{x})$  is taken to be a constant value above the melting temperature  $T_0(\mathbf{x}) = T_2 > T_m$ , modelling a region that is entirely in the liquid phase. For  $t \geq 0$ , the temperature at  $y = 0$  is set to a level  $T_1 < T_m$ , causing nucleation of a phase boundary. The analytical solution describing the subsequent motion of the phase front  $y_f$  is well known and given by

$$y_f(t) = 2\lambda\sqrt{\beta_1 t} \quad (48)$$

where  $\beta_1 = \kappa_1/c_1$  is the thermal diffusivity of the solid phase, and the constant  $\lambda$  satisfies the following relationship:

$$\frac{e^{-\lambda^2}}{\operatorname{erf}(\lambda)} = \frac{\kappa_2}{\kappa_1} \frac{\sqrt{\eta}(T_2 - T_m)e^{-\eta\lambda^2}}{(T_m - T_1)\operatorname{erfc}(\lambda\sqrt{\eta})} + \frac{\lambda L\sqrt{\pi}}{c_1(T_m - T_1)}$$

with  $\eta = \beta_1/\beta_2$  being the ratio of the thermal diffusivities. The temperature field in the solid phase  $y \leq y_f$  is then

$$T(\mathbf{x}) = T_1 + \frac{T_m - T_1}{\operatorname{erf}(\lambda)} \operatorname{erf}\left(\frac{y}{2\sqrt{\beta_1 t}}\right) \quad (49)$$

and in the liquid phase  $y \geq y_f$

$$T(\mathbf{x}) = T_2 - \frac{T_2 - T_m}{\operatorname{erfc}(\lambda\sqrt{\eta})} \operatorname{erfc}\left(\frac{y}{2\sqrt{\beta_2 t}}\right) \quad (50)$$

In the present investigation, we use the properties pertaining to water-saturated, dense sand provided in Reference [3] and listed in Table I.  $T_1$  and  $T_2$  were set to  $-10$  and  $4.0^\circ\text{C}$ . In this case,  $\lambda = 0.3073$ . We consider the case of an initial condition corresponding to  $t_0 > 0$  and the temperature field matching the exact solution given above. We simulate the evolution of the temperature field on  $\Omega = [0, 1] \times [0, 1]\text{cm}$ . To model an infinite domain, we fix the temperature to the exact solution at  $y = 1.0$ .

Table I. Numerical data of thermal properties of water saturated sand.

Properties	Phase		Interface
	Solid	Liquid	
Volumetric heat capacity ( $\text{cal}/^\circ\text{C cm}^3$ )	0.49	0.62	
Thermal conductivity ( $\text{cal}/\text{cm s }^\circ\text{C}$ )	$9.6 \times 10^{-3}$	$6.9 \times 10^{-3}$	
Melting temperature ( $^\circ\text{C}$ )			0.0
Volumetric latent heat of fusion ( $\text{cal}/\text{cm}^3$ )			19.2

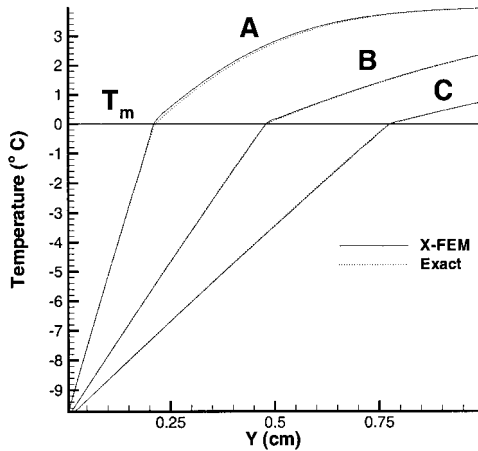


Figure 6. Comparison of exact and numerical solutions to the two-phase Stefan problem at times: A  $t = 6.31$  s, B  $t = 31.1$  s, and C  $t = 81.1$  s.

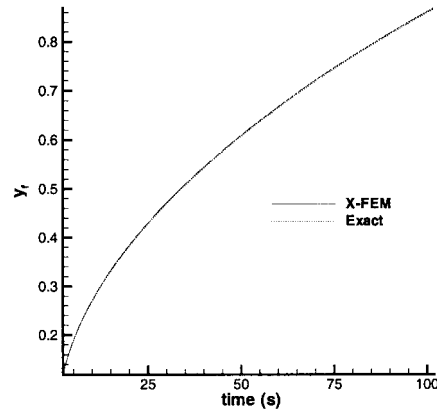


Figure 7. Comparison of X-FEM front position with exact solution.

The domain is partitioned into a  $20 \times 20$  uniform grid with elements of length  $h$ . For the underlying level set grid, a  $5 \times 5$  stencil is used in each finite element. In the following, we report results using  $\alpha = 1.0$  and  $\Delta t = 1.5h^2/\beta_1$ , where  $h$  is the nodal spacing in the finite element mesh. The results of the simulation are shown in Figure 6 at the three different times indicated. The enriched approximation is clearly capable of capturing the discontinuity in temperature gradient at the phase boundary, and an excellent agreement with the exact solution is obtained. Figure 7 shows the front position as a function of time for both the X-FEM and exact solution from (48). It bears emphasis that the phase boundary motion does not require the direct measurement of temperature gradients at the interface. Rather, the phase boundary velocity is determined from the jump in interfacial flux determined through the iterative procedure. Even with the relatively coarse finite element mesh, excellent agreement is obtained with the exact solution. Figure 8 plots the percent error in the front position in time. We observe less than 1% error over the entire period of time simulated.

As a means of comparison between the present formulation and one that employs a standard  $C^0(\Omega)$  approximation, we repeat the calculation with the approximation (11). A comparison of the error in the interface location with these results and the present formulation is shown in Figure 9. We observe that the  $C^1(\Omega)$  formulation is much more accurate with fewer total degrees of freedom. In particular, the results obtained with the  $C^1(\Omega)$  formulation and 385 degrees of freedom is more accurate than the  $C^0(\Omega)$  formulation with more degrees of freedom. The results seem to indicate that the present formulation is superior. We also note that the oscillations in the front position for the  $C^0(\Omega)$  formulation can be directly correlated with the interface passing an element boundary. By way of contrast, the present approach employing  $C^1(\Omega)$  polynomials appears far less sensitive.

In order to examine the convergence behaviour of the present approach, we conduct a series of calculations on increasingly refined meshes. All calculations are performed for 200 time

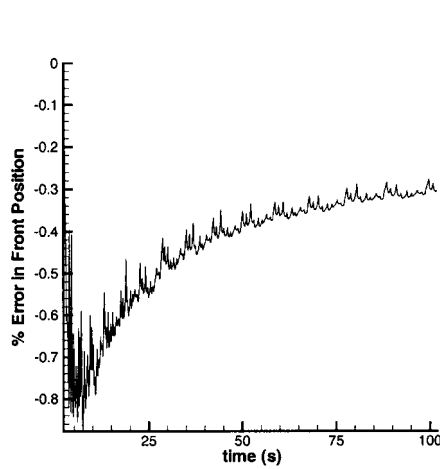


Figure 8. Per cent error in the front position with time.

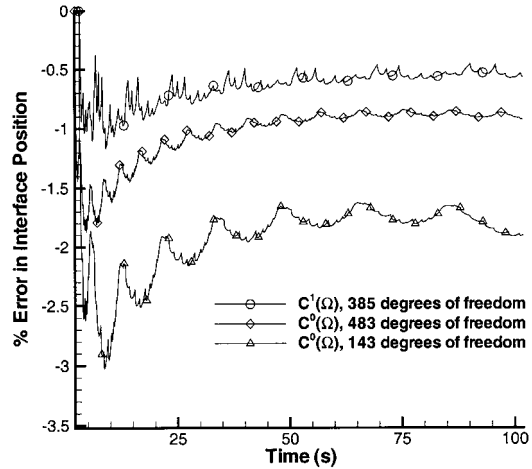


Figure 9. Per cent error in the front position with time for various approximations and grid sizes.

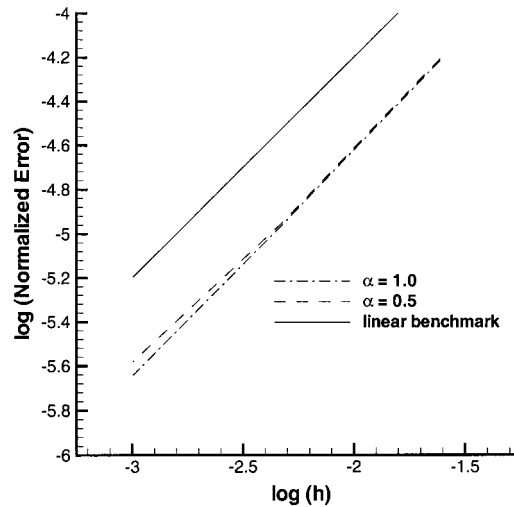


Figure 10. Convergence in the front position with grid refinement.

steps with the same time step size, with  $\alpha = 1.0$  and  $0.5$ . The results for the normalized error in the final front position are provided in Figure 10. The results indicate linear convergence in the front position for the coupled problem, for both choices of  $\alpha$ . This is not particularly surprising, as the speed function used in the Level Set method is only being calculated once per time step. In other words, we are effectively employing a Forward Euler time integration scheme for the interface position, and should not expect more than first-order accuracy. We

suspect that iteration on the front position within a time step may be necessary to obtain second order accuracy in the front position.

5.2. Solidification from a line heat sink

We consider the axisymmetric problem of solidification due to a continuous line heat sink located at the origin. The problem is a classical one in heat transfer, and its solution can be found in Reference [39]. We use  $R_f$  to denote the radius of the freezing front, and  $T_0 > T_m$  the initial temperature in the domain. At any time  $t > t_0$ , the temperature in the solid region  $r < R_f$  is given by

$$T(r, t) = T_m + \frac{Q}{4\pi\kappa_s} \left[ Ei \left( -\frac{r^2}{4\beta_s t} \right) - Ei(-\lambda^2) \right] \tag{51}$$

and in the liquid region  $r > R_f$  by

$$T(r, t) = T_0 - \frac{T_0 - T_m}{Ei(-\lambda^2\eta)} Ei \left( -\frac{r^2}{4\beta_l t} \right) \tag{52}$$

The position of the front is given by

$$R_f = 2\lambda\sqrt{\beta_s t} \tag{53}$$

In the above equations,  $\lambda$  is the root of the equation

$$\frac{Q}{4\pi} e^{-\lambda^2} = \lambda^2 \beta_s L - \frac{\kappa_l(T_0 - T_m)}{Ei(-\lambda^2\eta)} \tag{54}$$

and  $\eta$  is the ratio of thermal diffusivities;

$$\eta = \frac{\beta_s}{\beta_l} \tag{55}$$

The above solution is singular at the origin  $r = 0$ . We therefore adopt the approach employed in References [2, 7] of fixing the degrees of freedom at the center element according to the exact solution. By also fixing the exterior boundary conditions to match the exact solution, we may model an axisymmetric problem on a square domain. In the following, we report results for various non-dimensional *Stefan* numbers

$$St = \frac{c_s(T_0 - T_m)}{L}$$

We first present results for uniform material properties, i.e.  $\kappa_s = \kappa_l$ ,  $c_s = c_l$ , and a heat sink strength of 10.0. For this case,  $\lambda = 0.3669$ . Figure 11 compares the X-FEM and exact solutions for Stefan numbers of 1.0 and 0.1 on a uniform grid of  $21 \times 21$  quadrilateral elements covering a biunit square. For the numerical results, the average front radius is calculated for the comparison. In both cases, the results indicate less than 1% error in the front position over the entire time interval simulated. Figure 12 shows the intersection of the phase boundary with the uniform finite element grid. We emphasize that the mesh remains fixed throughout the computation.

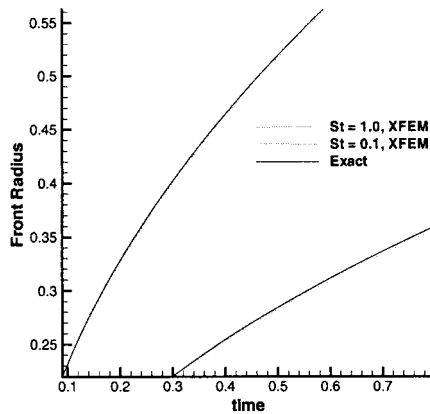


Figure 11. Comparison of X-FEM front radius to exact for the two-dimensional line heat sink problem.

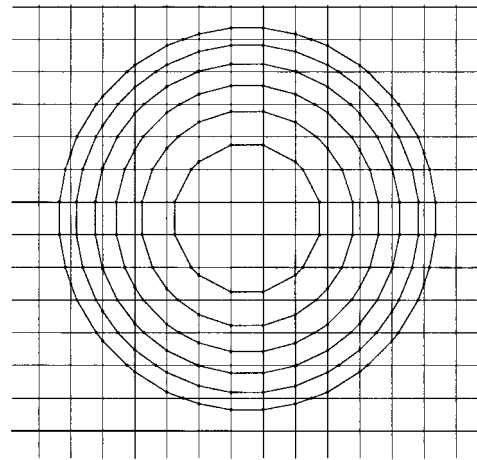


Figure 12. Intersection of the phase boundary with the computational grid at subsequent times for  $St=1.0$ .

Additional simulations with discontinuous material properties are performed with the same discretization, and the results are shown in Figure 13. We again observe less than 1% error in the location of the front. As a last example, we repeat the calculation for the case when  $\kappa_s/\kappa_l=0.2$  on a truncated domain and with slightly modified boundary conditions. In particular, we consider the evolution of an initially circular interface on the domain  $14/21 \times 2.0$ . Zero-flux boundary conditions are applied at both the left and right edge of the domain, and the temperature at the top and bottom surfaces is fixed to  $T=1.0$ . The initial temperature is taken to be that of the exact solution above for the size of the initial radius. Figure 14 shows the uniform background mesh and phase interface at equally spaced time intervals. The problem serves to demonstrate the utility of the Level Set approach in handling the topology change of the interface as it bifurcates from a simply-connected surface into two independent interfaces.

## 6. SUMMARY AND CONCLUDING REMARKS

A hybrid X-FEM/Level Set method has been presented for modelling phase transformations, with a particular focus on solidification problems. The method takes advantage of recent advances in enriched finite element approximations to represent a sharp interface on a fixed mesh. A new formulation was developed whereby classical Hermite polynomials were employed to generate a smooth partition of unity, and the approximation was enriched with a function possessing a discontinuous derivative across the interface. In order to represent the time derivative of the temperature field, an independent approximation with discontinuous enrichment was used in conjunction with a standard projection. A staggered strategy with the Level Set method was employed to describe the geometry of the interface and its evolution. Several numerical examples illustrated the excellent accuracy of the method, as well as the

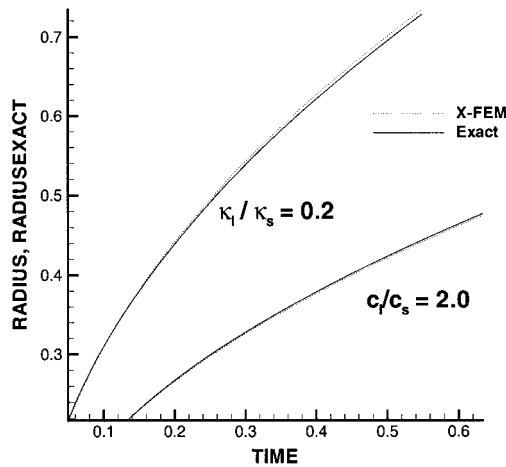


Figure 13. Comparison of results with discontinuous material properties.  $St = 1.0$ .

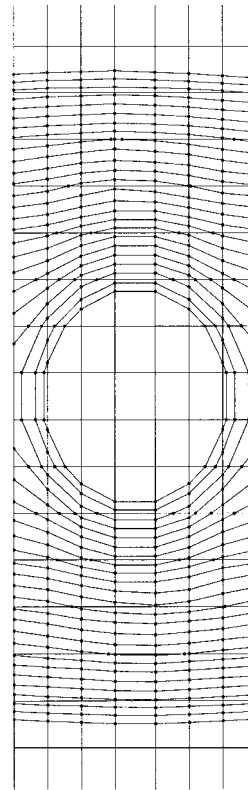


Figure 14. Evolution of phase interface on  $7 \times 21$  mesh.

advantage of the Hermite partition of unity. First-order accuracy in the front position was obtained for all problems investigated.

The method appears to possess a lot of potential and several areas for future work can be identified. The generalization of the present method to three dimensional problems is trivial. Research into dendritic solidification and more complex interfacial constraints is presently underway. Additional research may focus on obtaining second-order accuracy in the front position by subcycling with the Level Set method and the velocity of the phase interface within a given time step.

## APPENDIX A

The LATIN method [40] is a general procedure for solving non-linear problems in mechanics. Its iterative procedure marches between two sets of unknowns until convergence is achieved. The method was adopted in Reference [31] in conjunction with the X-FEM to model crack growth with frictional contact acting on the crack faces. In contrast to Lagrange multipliers,

it does not increase the size of the global system of equations, and is similar to the method of augmented Lagrangians developed by Simo and Laursen [41].

For the present problem, knowing all quantities at time  $t^n$ , we wish to determine the temperatures  $T^{n+1}$  and interface fluxes (5) at the new time step such that the weak form (21) is satisfied as well as the constraint (7). For notational clarity, we will drop the superscript  $n$  from all quantities, and assume the iterative procedure is invoked in moving from time step  $n$  to  $n + 1$ . We will also use subscripts  $m$  and  $m + 1$ , etc., to refer to iteration number. The iterative procedure adopted by the method begins by considering two sets of solution spaces. The variables of interest are the temperature  $T$ , its value on the interface  $\theta$ :

$$\theta = T|_{\Gamma_1} \quad (\text{A1})$$

and the heat fluxes on the interface (5). We use the compact notation:

$$v = (T, \theta, \bar{q}) \quad (\text{A2})$$

to define the solution spaces. Specifically, we let:

$$\mathbf{A}_d = \{v \text{ satisfying (21)}\}, \quad \mathbf{I} = \{v \text{ satisfying (7)}\} \quad (\text{A3})$$

We will use the superscript  $A$  and  $I$  to denote an element  $v$  in  $\mathbf{A}_d$  or  $\mathbf{I}$ , respectively.

The goal is then to find the element  $v^{AI}$  located at the intersection of  $\mathbf{A}_d$  and  $\mathbf{I}$ . Two successive approximations are always tied by a given search direction. The direction used when going 'down' from the set  $\mathbf{A}_d$  to the set  $\mathbf{I}$  is denoted by  $\mathbf{E}^{AI}$  whereas the direction when going 'up' from  $\mathbf{I}$  to  $\mathbf{A}_d$  is denoted by  $\mathbf{E}^{IA}$ . The two steps of the method are described in the following subsections.

#### A.1. The local step: update on the interface

The local update involves determining a new estimate  $v_m^I$  for the fluxes and temperatures on the interface given quantities obtained from a solution  $v_m^A \in \mathbf{A}_d$ . The new approximation is required to satisfy the constraint (i.e.  $v_m^I \in \mathbf{I}$ ). Additional equations are provided by the search direction.

To move from an element  $v_m^A \in \mathbf{A}_d$  to  $v_m^I \in \mathbf{I}$ , the search direction  $\mathbf{E}^{AI}$  is associated with a linear operator  $k_0$ . The search equations are then  $(v_m^I - v_m^A) \in \mathbf{E}^{AI} \Rightarrow$

$$\bar{q}_m^I - \bar{q}_m^A = k_0(\theta_m^I - \theta_m^A) \quad \text{on } \Gamma_1 \quad (\text{A4})$$

The process of determining  $v_m^I$  given  $v_m^A$  then involves solving the above search equation in conjunction with the constraint on the interface

$$v_m^I \in \mathbf{I} \Rightarrow \theta_m^+ = \theta_m^- = T_m \quad \text{on } \Gamma_1 \quad (\text{A5})$$

The resulting closed form equations for  $(\bar{q}_m^I, \theta_m^I)$  are very simple in this case. They are given by

$$\theta_m^{I+} = \theta_m^{I-} = T_m \quad (\text{A6a})$$

$$\bar{q}_m^I = \bar{q}_m^A + k_0(\theta_m^I - \theta_m^A) \quad (\text{A6b})$$

*A.2. The global step and error calculation*

We wish to move from  $v_m^l \in \mathbf{I}$  to  $v_{m+1}^A \in \mathbf{A}_d$ . This is accomplished through a global solve in conjunction with additional equations provided by the search direction  $\mathbf{E}^{LA}$  which is also associated with the  $k_0$  operator on the interface. With a known element  $v_m^l$ , the search equations are then

$$(v_{m+1}^A - v_m^l) \in \mathbf{E}^{LA} \Rightarrow \bar{q}_{m+1}^A - \bar{q}_m^l = -k_0(\theta_{m+1}^A - \theta_m^l) \quad \text{on } \Gamma_1 \tag{A7}$$

This equation is used in conjunction with the weak form of the governing equations (21), by solving for  $\bar{q}_{m+1}^A$  and making the substitution in the surface integrals on  $\Gamma_1$ . This yields

$$\begin{aligned} (w, cT_{m+1}^{n+1})_\Omega + \alpha \Delta t B(w, T_{m+1}^{n+1}) + \alpha \Delta t (w, k_0 T_{m+1}^{n+1})_{\Gamma_1} \\ = \alpha \Delta t (w, \bar{q}_m^l + k_0 \theta_m^l)_{\Gamma_1} + (w, cT^n)_\Omega + (1 - \alpha) \Delta t (w, cT_i^n)_\Omega \end{aligned} \tag{A8}$$

After solving (A8), the jump in the flux on the interface at step  $m + 1$  is given by

$$\bar{q}_{m+1}^A = \bar{q}_m^l + k_0(\theta_m^l - \theta_{m+1}^A) \tag{A9}$$

The search directions for the global and local steps, Equations (A4) and (A7), are conjugated i.e. expressed up to a sign by the same linear operator  $k_0$ . This ensures the convergence of the iterative strategy provided  $k_0$  is symmetric positive definite and some conditions on the material operator  $\mathcal{G}$  described in Ladev ze [40] are satisfied. In this paper,  $k_0$  is strictly positive and has the dimension of a thermal diffusivity over a length. We have obtained good results with the value

$$k_0 = \frac{\max(\kappa_i)}{L_0 \min(c_i)}$$

where  $L_0$  is a characteristic length for the domain.

The error indicator of convergence is computed after each global solve as the distance between the current and previous approximations:

$$\eta^2 = \frac{\|v_{m+1}^A - v_m^l\|^2}{\|v_{m+1}^A\|^2 + \|v_m^l\|^2} \tag{A10}$$

with the norm

$$\|v\|^2 = (\bar{q}, k_0^{-1} \bar{q})_{\Gamma_1} + (\theta, k_0 \theta)_{\Gamma_1} \tag{A11}$$

When the indicator  $\eta$  is below some tolerance, the iteration process is stopped. Note that if  $\eta = 0$ ,  $v_{m+1}^A = v_m^l$  is the exact solution. Finally, concerning the initialization, the solution  $v_0^A$  is built by solving the global step, Equations (A8)–(A9), with  $\bar{q}_m^l = \theta_m^l = 0$  and setting  $v_0^A = (T_m, \theta_m, \bar{q}_m)$ . In the iterative procedure to satisfy the constraints on the phase boundary, we found that a value of  $20k_0$  resulted in less than 15 iterations to provide a 1% error for the initial time step. In subsequent time steps, we have found that convergence is considerably accelerated by initializing  $v_0^l$  to the values obtained at the end of the previous iteration.

In order to numerically integrate the terms in (A8) on  $\Gamma_1$ , Gauss quadrature points are used along each of the one-dimensional subelements. The fields  $\theta$  and  $\bar{q}$  are then interpolated discretely, leading to a list of pairs  $(\bar{q}_g, \theta_g)_{g=1}^{n_g}$  on  $\Gamma_1$  where  $n_g$  is the total number of Gauss points on the interface. In the present investigation, we employ a two-point Gauss rule within each subelement. We note that in the special case when the interface aligns with the element edges, this strategy reduces to the traditional approach described in Reference [42].

#### ACKNOWLEDGEMENTS

The authors would like to thank Professor Nicolas Moës, of the Mechanical Engineering Department at the Ecole Centrale de Nantes, for his comments and suggestions concerning an early preprint of this manuscript. The authors are also very thankful to Professor N. Sukumar, of the University of California, Davis, for providing the C++ routines linking the X-FEM and level set codes.

#### REFERENCES

- Lewis R, Ravindran K. Finite element simulation of metal casting. *International Journal for Numerical Methods in Engineering* 2000; **47**:29–59.
- Juric D, Tryggvason G. A front tracking method for dendritic solidification. *Journal of Computational Physics* 1996; **123**:127–148.
- Lynch D, O’Neill K. Continuously deforming finite elements for the solution of parabolic problems, with and without phase change. *International Journal for Numerical Methods in Engineering* 1981; **17**:81–96.
- Sampath R, Zabaras N. An object oriented implementation of a front tracking finite element method for directional solidification processes. *International Journal for Numerical Methods in Engineering* 1999; **44**:1227–1265.
- Ghosh S, Moorthy S. An arbitrary Lagrangian–Eulerian finite element model for heat transfer analysis of solidification processes. *Numerical Heat Transfer: Part B* 1993; **23**:327–350.
- Leveque R, Li Z. Immersed interface method for elliptic equations with discontinuous coefficients and singular sources. *SIAM Journal on Numerical Analysis* 1994; **31**(4):1019–1044.
- Udaykumar H, Mittal R, Shyy W. Computation of solid–liquid phase fronts in the sharp interface limit on fixed grids. *Journal of Computational Physics* 1999; **153**:535–574.
- Melenk JM, Babuška I. The partition of unity finite element method: basic theory and applications. *Computer Methods in Applied Mechanics and Engineering* 1996; **39**:289–314.
- Moës N, Dolbow J, Belytschko T. A finite element method for crack growth without remeshing. *International Journal for Numerical Methods in Engineering* 1999; **46**:131–150.
- Dolbow J. An extended finite element method with discontinuous enrichment for applied mechanics. *Ph.D. Thesis*, Northwestern University, 1999.
- Belytschko T, Black T. Elastic crack growth in finite elements with minimal remeshing. *International Journal for Numerical Methods in Engineering* 1999; **45**:601–620.
- Daux C, Moës N, Dolbow J, Sukumar N, Belytschko T. Arbitrary branched and intersecting cracks with the extended finite element method. *International Journal for Numerical Methods in Engineering* 2000; **48**:1741–1760.
- Belytschko T, Moës N, Parimi C. Arbitrary discontinuities in finite elements. *International Journal for Numerical Methods in Engineering* 2001; **50**:993–1013.
- Dolbow J, Moës N, Belytschko T. Discontinuous enrichment in finite elements with a partition of unity method. *Finite Elements in Analysis and Design* 2000; **36**:235–260.
- Sukumar N, Moës N, Moran B, Belytschko T. Extended finite element method for three-dimensional crack modeling. *International Journal for Numerical Methods in Engineering* 2000; **48**(11):1549–1570.
- Strouboulis T, Copps K, Babuška I. The generalized finite element method: an example of its implementation and illustration of its performance. *International Journal for Numerical Methods in Engineering* 2000; **47**(8):1401–1417.
- Duarte C, Hamzeh O, Liska T. A generalized finite element method for the simulation of three-dimensional dynamic crack propagation. *Computer Methods in Applied Mechanics and Engineering* 2001; **190**:2227–2262.
- Sukumar N, Chopp D, Moës N, Belytschko T. Modeling holes and inclusions by level sets in the extended finite element method. *Computer Methods in Applied Mechanics and Engineering* 2001; **190**:6183–6200.
- Stolarska M, Chopp D, Moës N, Belytschko T. Modeling crack growth by level sets and the extended finite element method. *International Journal for Numerical Methods in Engineering* 2001; **51**:943–960.

20. Sukumar N, Chopp D, Moran B. Extended finite element method and fast marching method for three-dimensional fatigue crack propagation. *Engineering Fracture Mechanics*, 2001, accepted for publication.
21. Rao V, Hughes T, Garikipati K. On modeling thermal oxidation of Silicon II: numerical aspects. *International Journal for Numerical Methods in Engineering* 2000; **47**:359–377.
22. Simo J, Oliver J, Armero F. An analysis of strong discontinuities induced by softening solutions in rate-independent solids. *Journal of Computational Mechanics* 1993; **12**:277–296.
23. Dolbow J, Merle R. Modeling dendritic solidification with the extended finite element method. In *Proceedings of the First MIT Conference on Computational Fluid and Solid Mechanics*, Boston, 2001.
24. Merle R, Dolbow J. Solving thermal and phase change problems with the extended finite element method. *Computational Mechanics*, 2002, in press.
25. Chessa J, Smolinski P, Belytschko T. The extended finite element method for Stefan problems. *International Journal for Numerical Methods in Engineering* 2001; **52**:1959–1977.
26. Lynch D, Sullivan J. Heat conservation in deforming element phase change simulation. *Journal of Computational Physics* 1985; **57**:303–317.
27. Krongauz Y, Belytschko T. EFG approximation with discontinuous derivatives. *International Journal for Numerical Methods in Engineering* 1998; **41**(7):1215–1233.
28. Cirak F, Ortiz M, Schröder P. Subdivision surfaces: A new paradigm for thin-shell finite-element analysis. *International Journal for Numerical Methods in Engineering* 2000; **47**(12):2039–2072.
29. Gerlach C. Computational methods for the dynamic response of cracked specimen. *Ph.D. Thesis*, Northwestern University, 1999.
30. Froncioni A, Labbe P, Garon A, Camarero R. Interpolation-free space–time remeshing for the burgers equation. *Communications in Numerical Methods in Engineering* 1997; **13**:875–884.
31. Dolbow J, Moës N, Belytschko T. An extended finite element method for modeling crack growth with frictional contact. *Computer Methods in Applied Mechanics and Engineering* 2001; **190**(51–52):6825–6846.
32. Osher S, Sethian J. Fronts propagating with curvature dependent speed: algorithms based on Hamilton–Jacobi formulation. *Journal of Computational Physics* 1988; **79**:12–49.
33. Sethian JA. Numerical methods for propagating fronts. In *Variational Methods for Free Surface Interfaces*, Concus P, Finn R (eds). Springer: New York, 1987; 155–164.
34. Sethian JA. *Level Set Methods: Evolving Interfaces in Geometry, Fluid Mechanics, Computer Vision and Material Science*. Cambridge University Press: Cambridge, 1996b.
35. Chopp DL. Some improvements of the fast marching method. *SIAM Journal on Scientific Computing* 2001; **23**(1):230–244.
36. Sethian J. A marching level set method for monotonically advancing fronts. 1996a; **93**(4):1591–1595.
37. Sethian J. Fast marching methods. *SIAM Review* 1999; **41**(2):199–235.
38. Adalsteinsson D, Sethian JA. The fast construction of extension velocities in level set methods. *Journal of Computational Physics* 1999; **148**(1):2–22.
39. Carslaw H, Jaeger J. *Conduction of Heat in Solids*. Clarendon Press: Oxford, 1959.
40. Ladevèze P. *Nonlinear Computational Structural Mechanics*. Springer: New York, 1998.
41. Simo J, Laursen T. An augmented Lagrangian treatment of contact problems involving friction. *Computers and Structures* 1992; **42**:97–116.
42. Champaney L. Une Nouvelle Approche Modulaire Pour L’analyse D’assemblages de Structures Tridimensionnelles. *Ph.D. Thesis*, L’Ecole Normale Supérieure De Cachan, 1996.